Journal of Rock Mechanics and Geotechnical Engineering 18 (2026) 3882–3890

Contents lists available at ScienceDirect

Journal of Rock Mechanics and Geotechnical Engineering

journal homepage: www.jrmge.cn

Full Length Article

Anisotropic mechanical behaviour of Callovo-Oxfordian claystone under triaxial lateral unloading

Hao Wang [a,*], Yu-Jun Cui [a], Patrick Dangla [a], Minh Ngoc Vu [b], Jean Talandier [b]

[a] Laboratoire Navier/CERMES, Ecole des Ponts ParisTech, 6 et 8 avenue Blaise Pascal, Marne La Vallée cedex 2, 77455, France
[b] R&D Department, Andra, 92290, Châtenay-Malabry, France

ARTICLE INFO

Article history:
Received 16 March 2025
Received in revised form
16 July 2025
Accepted 1 September 2025
Available online 22 October 2025

Keywords:
Callovo-Oxfordian claystone
Triaxial unloading
Anisotropy
Young's modulus
Shear strength
Cigéo

ABSTRACT

Callovo-Oxfordian (COx) claystone has been selected as the host rock formation for the deep geological disposal of radioactive waste in France, called the Cigéo project. The excavation of drifts in the COx formation induced damage zones with an anisotropic shape, while the stress state around the drifts is almost isotropic. This is due to the anisotropic properties of the host rock formation and the instability caused by the brittle damage. In this study, the mechanical anisotropy of COx claystone was investigated through a triaxial shear test, where the axial stress was maintained while the lateral stress was decreased. Such a method was proposed for simulating one of the possible unloading paths involved during the excavation. The triaxial samples were prepared along different directions based on the angle between the axial loading direction and the one perpendicular to the bedding plane. Results show that the stress-strain curve exhibited an elasto-plastic pattern. With increasing deviatoric stress, a minor decline in Young's modulus E was observed, suggesting progressive damage behaviour. The shear strength changed with increasing the loading angle, showing the anisotropic property of COx claystone. Moreover, the results in this study and collected from other works show a time-dependent behaviour of COx claystone. It is attributed to the coupled effect of creep and pore pressure dissipation inside claystone.

1. Introduction

The Callovo-Oxfordian (COx) claystone has been designated in France as the host rock for the Cigéo deep geological repository of radioactive waste. Excavation of the disposal galleries induces fracturing in the COx claystone, forming an excavation damaged zone (EDZ) (Armand et al., 2014). Such damage may accelerate gallery convergence and pose potential risks to the repository's safety during its operational stage (Armand et al., 2013, 2017a; de La Vaissière et al., 2015). The size and geometry of the EDZ are influenced by the alignment of the drift relative to the orientation of the horizontal principal stresses (Armand et al., 2014). Drift excavations oriented along the major horizontal stress direction, under conditions of weakly anisotropic initial stresses, tend to generate an EDZ with strong lateral expansion and comparatively minor vertical development. The COx claystone, due to its sedimentary origin, possesses bedding-related anisotropy resulting from preferential grain alignment (Armand et al., 2017b; Zhang et al., 2019). This anisotropy exerts significant control on both its inherent properties and its reactions to thermo-hydro-mechanical changes (Conil et al., 2020; Bumbieler et al., 2021, 2024; Vu et al., 2023; Plúa et al., 2024). Computational approaches demonstrate that a realistic reproduction of the EDZ geometry requires explicit consideration of such anisotropic mechanical behaviour (Seyedi et al., 2017; Yu et al., 2021; Corman et al., 2022; Mánica et al., 2022a, 2022b; Souley et al., 2022, 2024). Therefore, repository design must incorporate these anisotropic effects, especially regarding EDZ formation.

Extensive laboratory investigations have been performed to evaluate the influence of anisotropy on the mechanical behaviour of COx claystone (Zhang and Rothfuchs, 2004; David et al., 2007; Zhang et al., 2010, 2012, 2019; Yang et al., 2013; Belmokhtar, 2017). Results show that thermal conductivity, permeability, swelling, self-sealing and creep are strongly controlled by

* Corresponding author.
E-mail address: hao.wang@enpc.fr (H. Wang).

Peer review under responsibility of Institute of Rock and Soil Mechanics, Chinese Academy of Sciences.

https://doi.org/10.1016/j.jrmge.2025.09.006

anisotropic features. Field observations further indicate that fracture patterns are also dependent on bedding orientation and distance from excavation surfaces (Armand et al., 2014). To capture these effects, Zhang et al. (2012) carried out micro-indentation and mini-compression experiments on samples exposed to varying humidity, while Zhang et al. (2019) examined specimens drilled at different angles to bedding using triaxial compression/extension, cyclic loading and creep tests. These studies revealed that deformability and strength are direction-dependent. Additionally, during excavation, the actual stress path is complex due to the complexity of in-situ stresses and rock properties, as illustrated in Fig. 1. The minimum radial stress σ_r consistently decreases, whereas the maximum axial stress σ_a may either drop, rise or remain unchanged (Huang et al., 2001; Li et al., 2017). Such stress paths may drive the deviatoric stress to critical levels, leading to wall damage. For the COx claystone, the constant confining pressure (CC) triaxial test was already carried out to explore the mechanical properties (e.g., Liu and Shao, 2016). Similarly, the constant mean stress (CM) loading path has been used for COx claystone, representing the stress conditions around deep tunnels when plane strain and isotropic elasticity are assumed (Liu et al., 2019). In these studies, although there were already some investigations on the unloading effect on the mechanical behaviour of COx claystone, for instance (Liu et al., 2019; Wang et al., 2022), it appears that the mechanical behaviour under the unloading path has not been fully explored, in particular while accounting for its anisotropic property.

As aforementioned, previous studies were conducted only under typical triaxial loading conditions, for instance, CC by Yang et al. (2013) and CM by Liu et al. (2019). In this study, a lateral unloading approach is proposed, where the confining pressure is reduced while axial stress remains constant. Triaxial tests on COx claystone are conducted under this path with cyclic loading. The Young's modulus is derived to assess both damage and anisotropic behaviour. The findings are then interpreted using an anisotropic strength model to describe the variation of shear strength with loading orientation.

2. Material and methods

2.1. Material

The COx claystone specimens were obtained from the Meuse/Haute-Marne Underground Research Laboratory (MHM URL) in France at a depth of about 490 m. At this level, in-situ stresses are ~12.7 MPa vertically, 12.7–14.8 MPa in the major horizontal direction, and ~12.4 MPa in the minor horizontal direction, with a pore water pressure of 4.7 MPa (Wileveau et al., 2007). The rock has a specific gravity of 2.7 (Zhang et al., 2019). To limit desaturation and deformation, the cores were preserved in a fully confined cell (T1) and sealed with a membrane, with dimensions of 80 mm in diameter and 300 mm in length. Mineralogically, the COx claystone is composed of approximately 45 %–50 % clay minerals (illite-smectite, illite, kaolinite, chlorite, etc.), 20 %–30 % carbonates, and 20 %–30 % quartz (Gaucher et al., 2004).

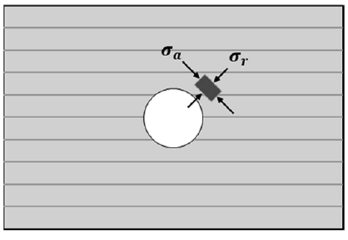

Fig. 1. Stress state illustrated in the vicinity of the excavation face.

2.2. Sample preparation

After opening the confined cell (T1), triaxial samples of COx claystone, measuring 38 mm in diameter and 65 mm in height, were extracted from the T1 core using a drilling machine. Both ends of each sample were then trimmed with a diamond wire to achieve flat surfaces. The procedure for sample preparation is illustrated in Fig. 2. Previous research has indicated that COx claystone exhibits transverse isotropy (Zhang et al., 2019). To examine the anisotropic behaviour, triaxial samples were carefully prepared by drilling in various orientations relative to the bedding plane (illustrated by grey parallel lines in Fig. 2). The bedding plane direction was marked on the surface of the COx claystone core when it was drilled under in-situ conditions. Besides, the direction was also confirmed by immersing a small piece of claystone into distilled water to observe the cracking direction. $\theta = 0^o$ corresponds to the axial direction normal to the bedding plane, whereas $\theta = 90^o$ represents the direction parallel to it. Additionally, the initial physical properties were assessed immediately after the T1 cell was opened, and the results are presented in Table 1. It should be noted that the initial total suction was determined using a Decagon WP4 dew point tensiometer, and small fragments were cut and oven-dried at 105 °C to determine the water content. The porosity (void ratio) and degree of saturation were obtained by measuring the volume (see Menaceur et al. (2016) for more details). During the preparation of samples, the cores were consistently wrapped in plastic film to minimise the water loss.

2.3. Experimental methods

In the present study, a high-pressure triaxial testing system was employed (Fig. 3). The maximum confining pressure, regulated by a pressure-volume controller (PVC), reached 64 MPa. Axial force was monitored using a 100 kN capacity force sensor, while local axial and radial deformations were measured with Linear Variable Differential Transformers (LVDTs) offering a resolution of 0.0001 mm. The lateral strains in the two horizontal directions were measured through four horizontal LVDT stems, as displayed in Fig. 4.

The underground excavation in COx claystone involves complex changes in stress state. In this work, the anisotropic mechanical behaviour was examined using a drained triaxial unloading path (CA), in which the confining pressure was gradually reduced while maintaining a constant axial stress. The stress change in the p-q plane during deviatoric loading is illustrated in Fig. 5a. Compared to the loading paths CC and CM depicted in Fig. 5a, a decreasing tendency of mean stress is expected under the CA.

During the triaxial test, a filter paper and a porous disk were

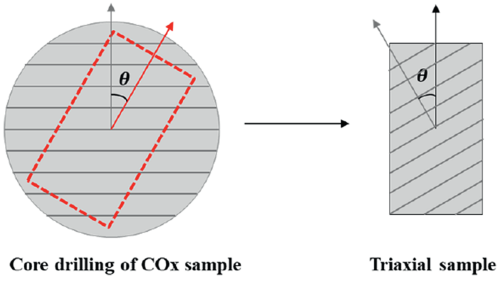

Fig. 2. Drilling and cutting process.

Table 1
Initial physical characteristics of claystone core.

Core ID	Density (g/cm^3)	Dry density (g/cm^3)	Porosity (%)	Water content (%)	Total suction (MPa)	Saturation degree (%)
EST58108	2.39	2.21	18.05	8.26	21.78	98.8

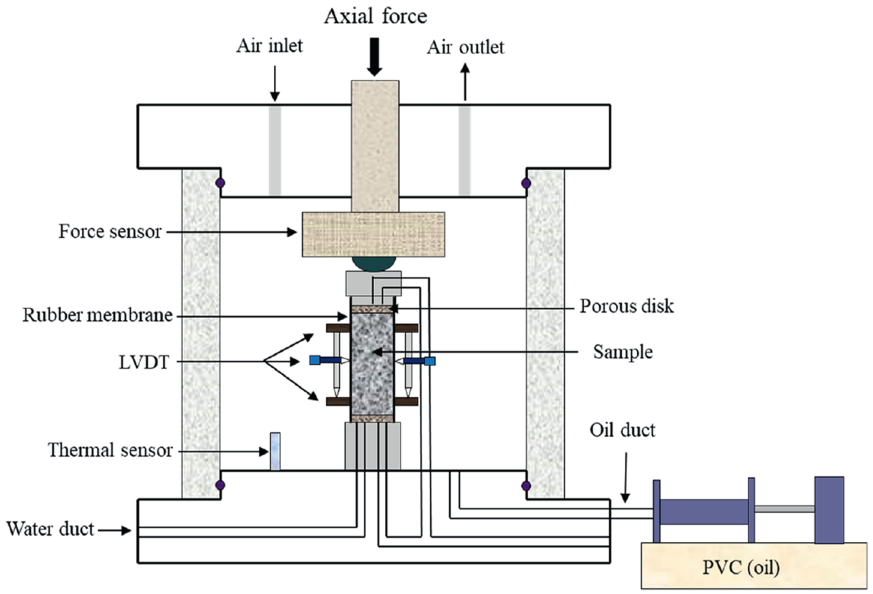

Fig. 3. Schematic illustration of high-pressure triaxial device.

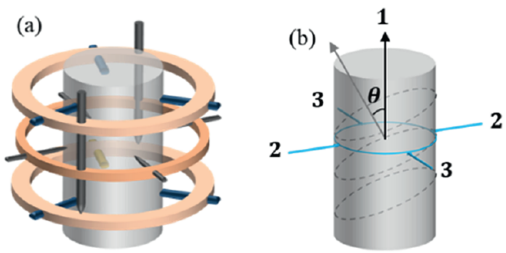

Fig. 4. Setup of LVDTs on triaxial sample.

placed between the sample ends and the top piston or bottom base. The sides of the sample were wrapped in a thin rubber membrane. In the whole testing process, there was no additional water injected into the triaxial cell. The samples kept the quasi-saturation state. Each triaxial specimen was first subjected to isotropic loading up to a target stress of 14 MPa, applied at rates of 5 kPa/min or 20 kPa/min to examine the influence of loading rate. Afterwards, the CA loading path was applied by changing the confining pressure at a rate of 5 kPa/min or 20 kPa/min 3 or 4 unloading and reloading cycles were conducted to assess the elastic properties. Fig. 5b illustrates the detailed loading process for the CA path, which includes both isotropic and deviatoric loadings. The test program is outlined in Table 2. While relative humidity is known to substantially affect the degradation of COx claystone (Wang et al., 2014, 2015), the present study focuses exclusively on the damage induced by unloading, without considering the effects of humidity.

In order to analyse the mechanical parameters, transversely anisotropic elasticity analysis was applied. The elastic parameters were determined to characterise their evolution during shearing. The results from the unloading-reloading cycles were used to calculate Young's moduli in various directions at different deviatoric stresses, based on Eq. (1) with consideration of different loading angles θ (according to Eq. (A11) in Appendix A). In Eq. (1), the first equation is derived by summing the first and second rows of Eq. (A11), while the second equation corresponds to the third row. Therefore, the Young's moduli along directions normal and parallel to the bedding plane can be directly obtained from the

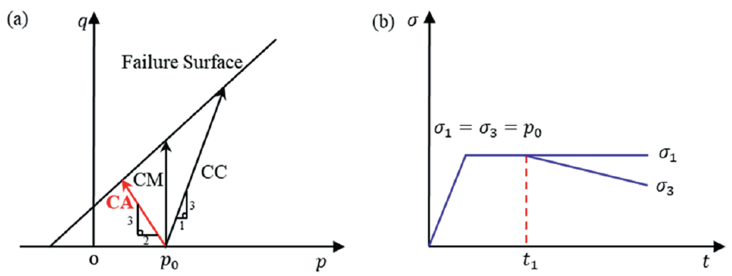

Fig. 5. (a) Loading paths CA, CM and CC in the p-q plane; (b) Loading path CA in the σ-t plane.

Table 2
Test program.

Test No.	Porosity (%)	Water content (%)	Saturation degree (%)	Unloading rate (kPa/min)	Loading direction (°)
CA1	18.1	8.1	98.9	20	0
CA2	17.8	7.9	98.5	5	0
CA3	17.9	7.9	97.8	20	30
CA4	17.8	7.8	97.2	20	45
CA5	18.0	8.1	99.6	20	60
CA6	18.1	8.0	97.7	20	90

measured strains in the three directions of the triaxial sample (Fig. 4 and Fig. A1), without accounting for shear strain effects. In this study, ν_{hh} and ν_{vh} are assumed to be 0.2 and 0.3, respectively, as reported by Zhang et al. (2019).

$$\left.\begin{aligned}\Delta\varepsilon_1+\Delta\varepsilon_2&=\frac{\Delta\sigma_3\sin^2\theta(1-\nu_{vh})}{E_v}+\frac{\Delta\sigma_3(\cos^2\theta-\nu_{hv}\cos^2\theta-\nu_{hv}-\nu_{hh})}{E_h}\\ \Delta\varepsilon_3&=-\frac{\nu_{vh}\Delta\sigma_3\sin^2\theta}{E_v}+\frac{\Delta\sigma_3(1-\nu_{hh}\cos^2\theta)}{E_h}\end{aligned}\right\}\tag{1}$$

3. Experimental results

3.1. Isotropic loading

Fig. 6 illustrates the evolution of various strains during isotropic loading up to 14 MPa at different loading rates. At this pressure, micro-cracks potentially generated during drilling and sawing are expected to close (Mohajerani et al., 2011; Zhang et al., 2019; Wang et al., 2022). At the initial stage of isotropic loading, the axial strains in tests CA1 and CA2 increase nonlinearly with the applied mean stress, suggesting the potential existence of micro-cracks within the samples. A similar observation was reported by Zhang et al. (2019), who attributed it to the closure of micro-cracks formed during sample preparation. The isotropic loading produces a nonlinear stress-strain response along the axial direction, with the bedding plane serving as the primary orientation for micro-crack opening (Chiarelli et al., 2003; Zhang et al., 2019). Furthermore, the strain ε_1 perpendicular to bedding is noticeably larger than ε_3 parallel to bedding, confirming the anisotropic nature of COx claystone. Additionally, a pronounced time-dependent strain effect is observed following isotropic loading, which can be attributed to both creep and the dissipation of excess pore pressure (Wang et al., 2022). The latter arises during isotropic loading due to the extremely low permeability of COx claystone, ranging from 5×10^{-20} m^2 to 5×10^{-21} m^2 (Armand et al., 2014).

3.2. Shear loading

Fig. 7 illustrates the variations of axial, lateral, and mean stresses as functions of axial and lateral strains in test CA1. As the lateral stress (confining pressure) decreases, the mean stress correspondingly declines, with the change in mean stress being approximately 2/3 of the variation in lateral stress. It appears that in the shearing process, the axial stress was well kept constant before the peak deviator stress, indicating that the stress path CA was well applied in the triaxial test.

Fig. 8 presents the stress-strain responses of tests CA1 and CA2

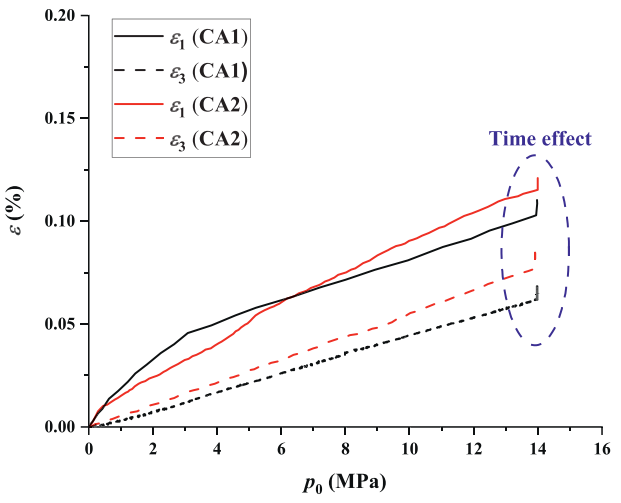

Fig. 6. Strains measured in axial and radial directions during isotropic loading.

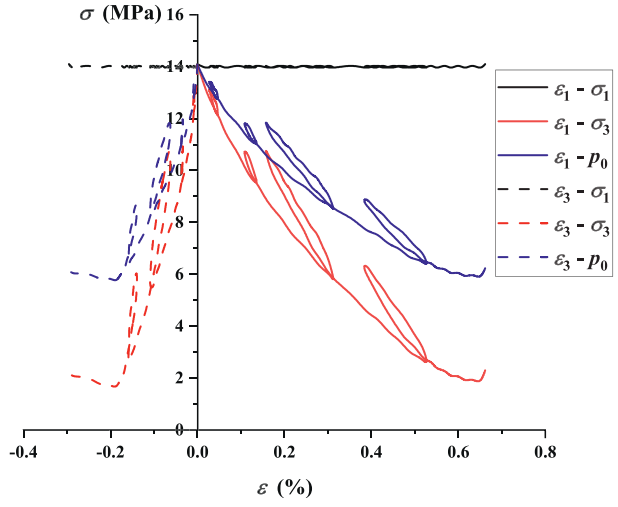

Fig. 7. Evolutions of stresses and strains in test CA1.

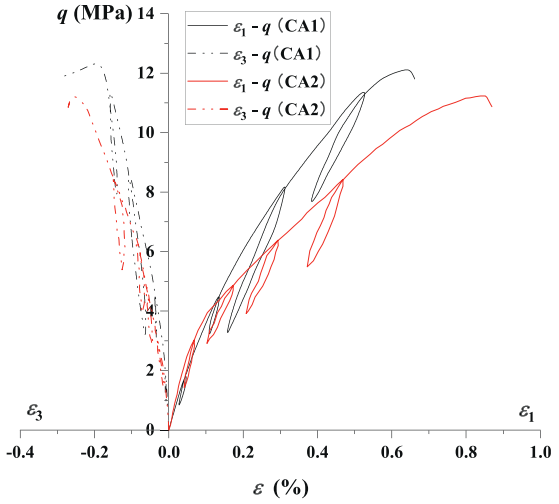

Fig. 8. Comparisons of stress-strain curves between tests CA1 and CA2.

under constant axial stress at $\theta = 0^{o}$. At the initial stage of loading, the curves are nearly linear, indicating an absence of micro-cracks. They gradually become nonlinear due to the combined influences of plastic deformation and damage (Le Pense et al., 2016; Bian et al., 2017). Both CA1 and CA2 samples, originating from the same core, have an identical water content of 8.26 %. Consequently, the peak deviatoric stresses, q_{max} (12.1 MPa and 11.2 MPa), are very close, though minor differences are still observed in their stress-strain behaviour. This difference may be related to the adopted isotropic loading rates. Indeed, a higher loading rate may result in a higher residual excess pore water pressure and a more significant time-dependent effect, thus a higher peak deviator stress.

The tests CA3, CA4, CA5 and CA6 were conducted under the same loading condition as tests CA1 and CA2, but at different loading angles ($\theta = 30^{o}$, $\theta = 45^{o}$, $\theta = 60^{o}$ and $\theta = 90^{o}$). The results are shown in Fig. 9. Overall, the stress-strain curves exhibit noticeable nonlinearity, permanent strain after unloading, and hysteresis during unloading–reloading cycles. The corresponding peak deviator stresses obtained are 11.1 MPa, 10.1 MPa, 11.5 MPa and 13.5 MPa. It is observed that as the loading angle increases, the peak deviator stress initially decreases and subsequently rises. The minimum and maximum peak deviator stresses correspond to the loading angle $\theta = 45^{o}$ and $\theta = 90^{o}$, respectively. This clearly indicates the strength anisotropy of COx claystone. Moreover, according to the development of two lateral strains measured in the tests, an obvious difference was observed, which confirms the mechanical anisotropy of COx claystone.

3.3. Failure mode

Fig. 10 presents the failure pictures from tests CA2 to CA6 after

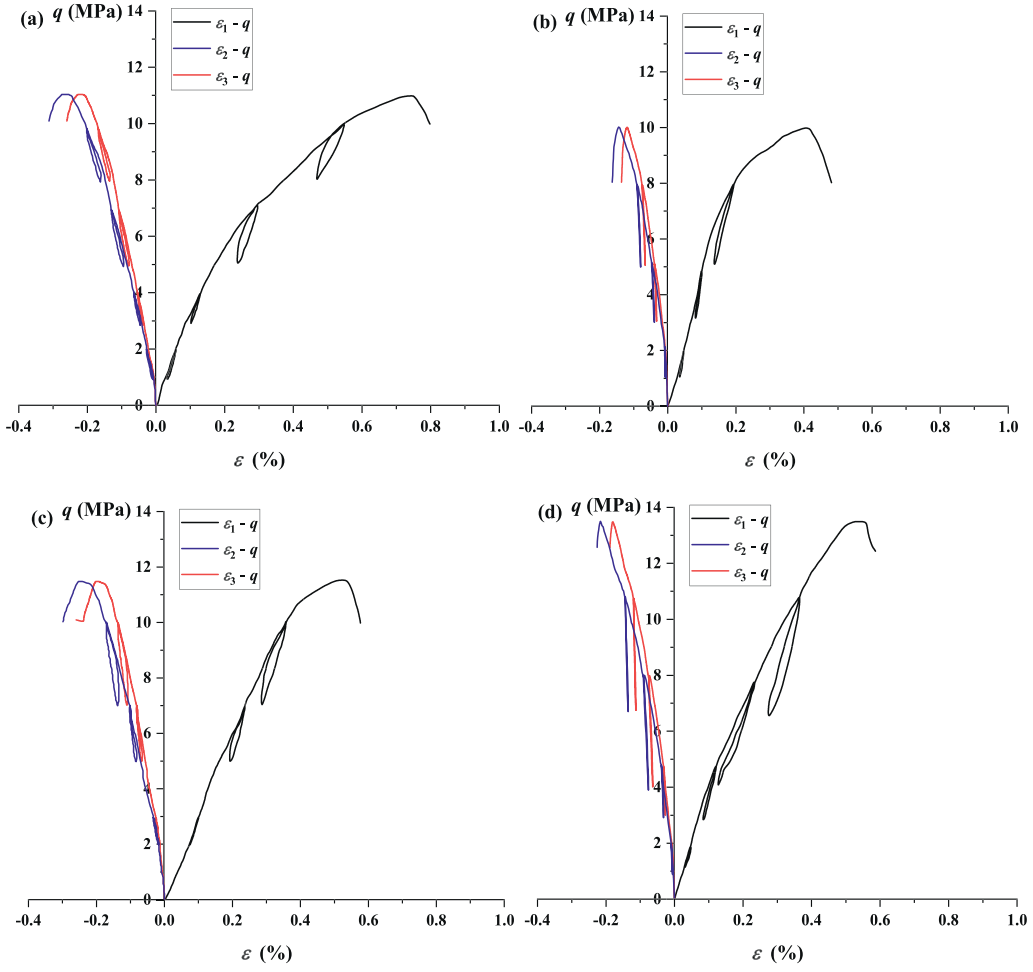

Fig. 9. Stress-strain curves at different loading angles: (a) test CA3 at $\theta = 30^{o}$; (b) test CA4 at $\theta = 45^{o}$; (c) test CA5 at $\theta = 60^{o}$; (d) test CA6 at $\theta = 90^{o}$.

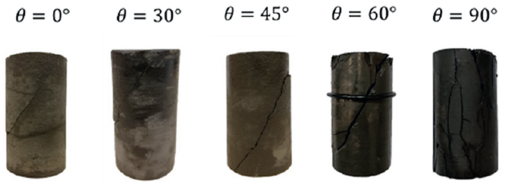

Fig. 10. Pictures of failed samples after triaxial shearing.

testing. During the shearing process, micro-cracks were generated progressively with the increase of deviator stress, then propagated, and finally formed a connection fracture. The major shear failure modes can be visually appreciated. The morphology and orientation of the cracks are similar to those observed in the conventional triaxial compression tests by Zhang et al. (2019). These findings suggest that cracking plays a key role in the deformation and failure of COx claystone (Liu et al., 2019). Qualitatively, the fracture angle—defined as the angle between the fracture surface and the horizontal direction—tends to increase as the loading angle θ becomes larger. As the loading angle increases, the main mode regarding failure changes from the shearing of bedding plane at $\theta = 0^{o}$, the sliding along bedding plane at $\theta = 45^{o}$ to the tensile splitting of bedding plane at $\theta = 90^{o}$. The fracture patterns observed in these tests align with in-situ observations of COx claystone (Zhang et al., 2019) and Tournemire shale (Niandou et al., 1997) under the loading path CC. This mechanical anisotropy should be considered when modelling the hydro-mechanical behaviour of the EDZ (Seyedi et al., 2017).

4. Analysis and discussion

4.1. Loading rate effect

To further reveal the anisotropy and time-dependent behaviour under isotropic loading, the data by Wang (2021) is collected as shown in Fig. 11a. For tests CC and CM, the adopted isotropic loading rate is 100 kPa/min. It is evident that the strain variations with increasing mean stress also exhibit anisotropic and nonlinear stress-strain behaviour, consistent with the findings of this study (Fig. 6). To analyse the time-dependent deformation after stopping isotropic loading, the time-strain curves of tests CA-1 and CA-2 are compared to the results at $\theta = 0^{o}$ collected from Wang (2021). Fig. 11b shows the comparisons between different tests, and a significant time-dependent behaviour is observed. Besides, for test CC at the loading rate of 100 kPa/min, as significant microcracks were generated in the sample preparation, a significant strain increase in the axial direction occurs due to crack closure. Interestingly, the creep deformation after stopping loading is also most significant (Wang et al., 2022). Overall, the time-dependent evolution of strains can be divided into two stages: (1) a rapid increase phase, primarily driven by the dissipation of excess pore pressure, and (2) a gradual, steady increase phase, mainly resulting from creep behaviour. For the comparisons of tests CM, CA-1, and CA-2, the loading rate decreases from 100 kPa/min to 5 kPa/min, and the final time-dependent deformation also correspondingly decreases. It could be inferred that the higher loading rate results in the larger time-dependent deformation, mainly due to the accumulated excess pore water pressure during isotropic loading in a shorter time.

4.2. Analysis of Young's modulus

Using the data from unloading–reloading cycles, the Young's moduli (E_v and E_h) along directions normal and parallel to the

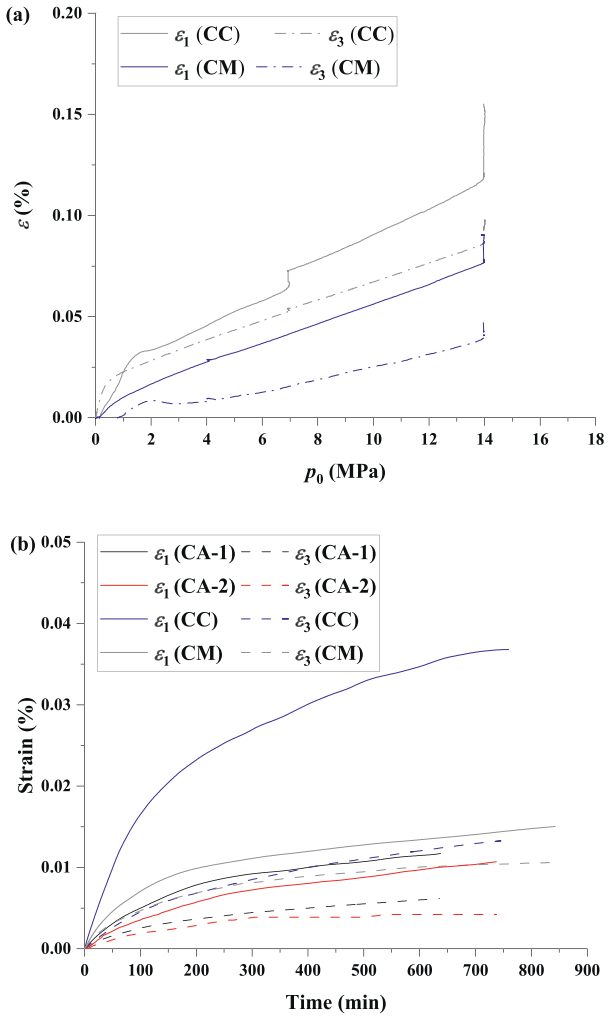

Fig. 11. (a) Isotropic stress-strain curves at 100 kPa/min by Wang (2021) and (b) time-strain curves from this study and Wang (2021).

bedding plane were calculated under the assumption of transverse isotropy. Fig. 12 illustrates the evolution of E_v and E_h with increasing normalised axial strain, $\varepsilon_1/\varepsilon_{1,max}$, based on the present study and previous works. Here, $\varepsilon_{1,max}$ represents the axial strain at the peak deviator stress. The data show slight scatter, but overall, both E_v and E_h exhibit a gradual decrease as normalised axial strain increases, indicating that shear loading contributes to the damage of COx claystone (Liu et al., 2019). Comparing E_v in Fig. 12a from this study under CA with values reported by Wang et al. (2022) and Armand et al. (2017b) under CC, it appears that with higher mean stress (see Fig. 5a), E_v is larger, highlighting the dependence of the elastic modulus on mean stress. In addition, by comparing the values of E_v and E_h in Fig. 12a and b, it can be observed that the values E_v are also slightly smaller than those of E_h at the same normalised axial strain, illustrating the elastic anisotropy of COx claystone.

4.3. Strength anisotropy

For assessing the strength anisotropy, the change of peak deviator stresses with increasing loading angle is plotted in Fig. 13. It is found that the maximum strength appears at $\theta = 90^{o}$, while the minimum one at $\theta = 45^{o}$. Eq. (2) is adopted to quantify the relationship between peak deviator stress and loading angle

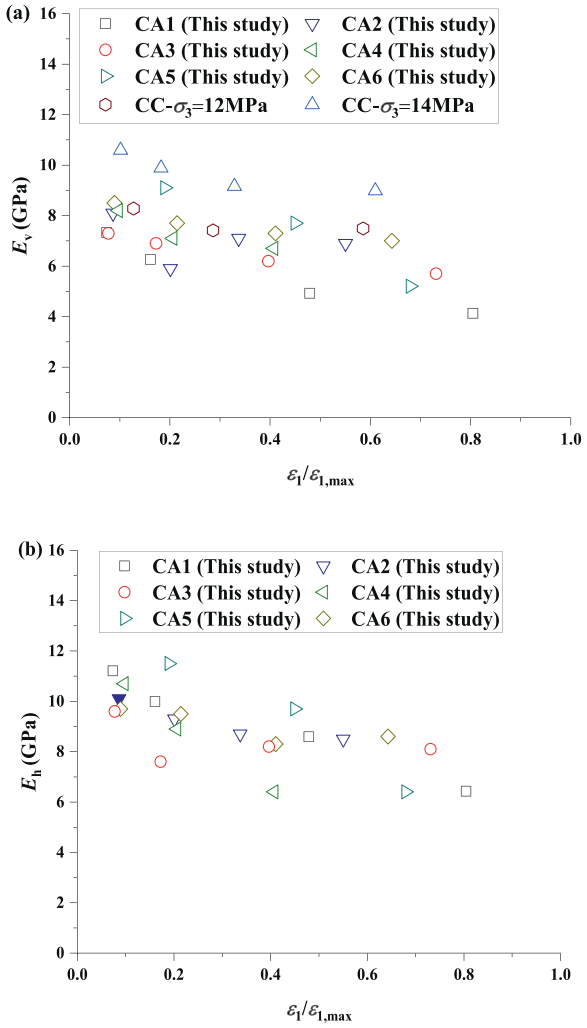

Fig. 12. Evolutions of Young's moduli with normalised axial strain: (a) E_v and (b) E_h. Note, data for CC tests under 12 MPa and 14 MPa are from Armand et al. (2017b) and Wang et al. (2022), respectively.

(Boehler and Sawczuk, 1974):

$$q_\theta / q_0 = \frac{1}{\sqrt{\left(\cos\theta^2 + r_1 \sin\theta^2\right)^2 + \left(2r_2{}^2 - 3r_1\right)\cos\theta^2 \sin\theta^2}} \quad (2)$$

where q_θ and q_0 are the peak deviator stresses at θ and $\theta = 0^o$ (i.e., the loading direction perpendicular to bedding plane); r_1 and r_2 represent the ratios of q_0/q_θ at $\theta = 90^o$ and $\theta = 45^o$, respectively.

By using the anisotropic strength model Eq. (2), a continuous evolution of peak deviator stress with loading angle is identified, as presented in Fig. 13. The changing tendency is in good accordance with the experimental observation. Besides, the changes in strength with loading angle reported by Souley et al. (2024) are collected in Fig. 14 and also quantitatively analysed with Eq. (2). It is found that due to the variability of COx claystone, the results are slightly scattered, but still show the obvious dependency of peak deviator stresses on loading angle. Moreover, the differences in loading conditions may also influence the strength anisotropy; for instance, the higher confining pressure could make the claystone more ductile. According to the determined upper and lower bounds, the values of parameters r_1 and r_2 are determined to be

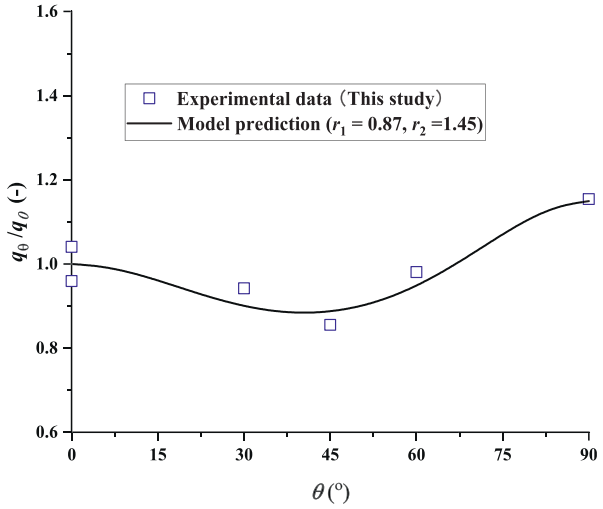

Fig. 13. Relationship between normalised shear strength and loading angle.

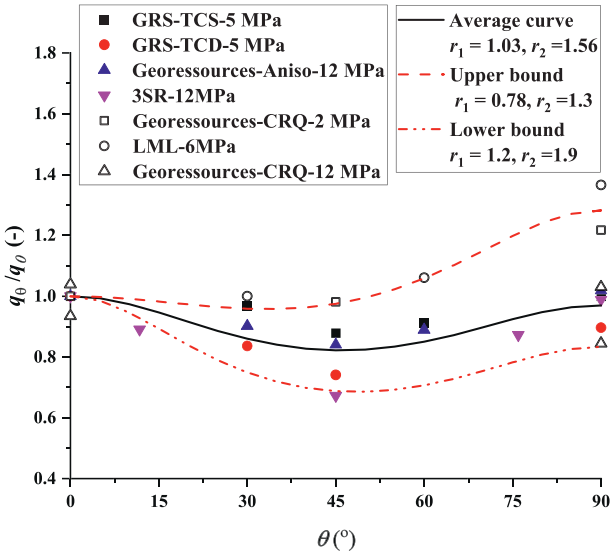

Fig. 14. Relationships between normalised shear strength and loading angle in other works (data from Souley et al., 2024).

0.78–1.20 and 1.30–1.90, which cover the values of 0.87 and 1.45 from this study.

4.4. Failure surface

In Fig. 15, the values of peak deviator stresses obtained under different loading paths, including CA in this study and CC, CM by Wang et al. (2022), are compared in the *p*-*q* plane. It appears that from the same stress state, the peak deviator stresses are quite different under different loading paths. The mean stress also decreases in the order of CM, CC and CA. Based on the Mohr-Coulomb criterion, a linear relationship between peak deviator stress and mean stress under different loading paths is determined. According to the strength data in Fig. 15, the friction angle and cohesion were determined: $\varphi' = 24.2^\circ$ and $c' = 3.91$ MPa, which are in the range found in the literature: $\varphi' = 19.62^\circ$–25° and $c' = 3.83$–7 MPa (Wileveau and Bernier, 2008; Hu et al., 2014; Zhang, 2016; Belmokhtar, 2017). It is worth noting that the nonlinear failure criterion, reported by Braun et al. (2022), may be more suitable for

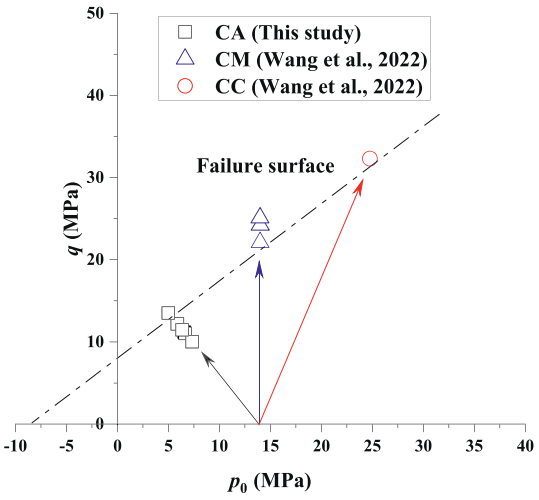

Fig. 15. Comparisons of peak deviator stresses obtained under different loading paths.

COx claystone with considering the dependency on stress paths observed in Fig. 15. The considerable scatter in the friction angle and cohesion values obtained from the linear criterion can be attributed to the nonlinear strength behaviour of COx claystone.

5. Conclusions

The mechanical behaviours of COx claystone were investigated by performing triaxial tests with lateral unloading while maintaining constant axial stress. For the purpose of exploring the anisotropy of COx claystone, triaxial samples were prepared along different directions in terms of the bedding plane. Based on the obtained experimental data, the elasticity and strength anisotropy, and failure behaviour were analysed. The main conclusions are drawn as follows:

During isotropic loading, the axial strain exceeds the lateral strain, reflecting the material's anisotropic nature. In addition, the rate of isotropic loading influences the subsequent volumetric change, resulting from pore pressure dissipation and creep effects. The stress-strain curve during shearing displayed elasto-plastic behaviour. Young's moduli measured both perpendicular and parallel to the bedding plane showed a decreasing trend throughout shearing, reflecting the progressive damage of the claystone. The anisotropic behaviour was also observed through the differences in the development of two lateral strains when the loading angle was not equal to 0°. The elastic anisotropy is reflected by lower moduli in the direction normal to the bedding plane compared to those parallel to it.

The strength decreases first with the increase of loading angle, then increases, showing the strength anisotropy. A strength anisotropy model was adopted to quantitatively evaluate the evolution of strength with the loading angle. The strength in the CA loading path is significantly smaller than that in CC and CM due to the lower mean stress, indicating that the strength is dependent on the mean stress and the loading direction with respect to the bedding.

CRediT authorship contribution statement

Hao Wang: Writing – original draft, Methodology, Investigation, Conceptualization. **Yu-Jun Cui:** Writing – review & editing, Supervision, Methodology, Conceptualization. **Patrick Dangla:** Writing – review & editing, Supervision. **Minh Ngoc Vu:** Writing – review & editing, Methodology. **Jean Talandier:** Writing – review & editing, Methodology.

Declaration of competing interest

The authors declare that they have no known competing financial interests or personal relationships that could have appeared to influence the work reported in this paper.

Appendix A. Supplementary data

Supplementary data to this article can be found online at https://doi.org/10.1016/j.jrmge.2025.09.006.

References

Armand, G., Noiret, A., Zghondi, J., Seyedi, D.M., 2013. Short- and long-term behaviours of drifts in the callovo-oxfordian claystone at the Meuse/Haute-Marne underground research laboratory. J. Rock Mech. Geotech. Eng. 5 (3), 221–230.

Armand, G., Leveau, F., Nussbaum, C., de La Vaissière, R., Noiret, A., Jaeggi, D., Landrein, P., Righini, C., 2014. Geometry and properties of the excavation-induced fractures at the Meuse/Haute-Marne URL drifts. Rock Mech. Rock Eng. 47 (1), 21–41.

Armand, G., Bumbieler, F., Conil, N., Cararreto, S., de La Vaissière, R., Noiret, A., Seyedi, D., Talandier, J., Vu, M.N., Zghondi, J., 2017a. The Meuse/Haute-Marne underground research laboratory: mechanical behavior of the Callovo-Oxfordian claystone. In: Feng, X.-T. (Ed.), Rock Mechanics and Engineering, vol. 2.

Armand, G., Conil, N., Talandier, J., Seyedi, D.M., 2017b. Fundamental aspects of the hydromechanical behaviour of Callovo-Oxfordian claystone: from experimental studies to model calibration and validation. Comput. Geotech. 85, 277–286.

Belmokhtar, M., 2017. Contributions À L'Étude Du Comportement thermo-hydro-mécanique De L'Argilite Du Callovo-Oxfordien (France) Et De L'Argile À Opalinus (Suisse). PhD Thesis. Université Paris-Est, France.

Bian, H., Zhang, X., Shao, J., 2017. A coupled elastoplastic and visco-plastic damage model for hard clay and its application for the underground gallery excavation. Undergr. Space 2 (1), 60–72.

Boehler, J.P., Sawczuk, A., 1974. Analyse géométrie des critères d'écoulement plastique anisotrope. In: Proceedings of the Rheology and Soil Mechanics/ Rhéologie Et Mécanique Des Sols Symposium.

Braun, P., Delage, P., Ghabezloo, S., Chabot, B., Conil, N., Vu, M.N., 2022. Inducing tensile failure of claystone through thermal pressurization in a novel triaxial device. Rock Mech. Rock Eng. 55 (7), 3881–3899.

Bumbieler, F., Plúa, C., Tourchi, S., Vu, M.N., Vaunat, J., Gens, A., Armand, G., 2021. Feasibility of constructing a full-scale radioactive high-level waste disposal cell and characterization of its thermo-hydro-mechanical behavior. Int. J. Rock Mech. Min. Sci. 137, 104555.

Bumbieler, F., Plúa, C., Vu, M.N., Armand, G., 2024. Assessment of a full-scale in-situ heater experiment based on the French high-level waste disposal cell concept conducted in the Callovo-Oxfordian claystone. Tunn. Undergr. Space Technol. 153, 106004.

Chiarelli, A.S., Shao, J.F., Hoteit, N., 2003. Modeling of elastoplastic damage behavior of a claystone. Int. J. Plast. 19 (1), 23–45.

Conil, N., Vitel, M., Plúa, C., Vu, M.N., Seyedi, D., Armand, G., 2020. In situ investigation of the THM behavior of the Callovo-Oxfordian claystone. Rock Mech. Rock Eng. 53, 2747–2769.

Corman, G., Vu, M.N., Collin, F., 2022. Numerical investigation of the couplings between strain localisation processes and gas migrations in clay materials. Int. J. Solid Struct. 256, 111974.

de La Vaissière, R., Armand, G., Talandier, J., 2015. Gas and water flow in an excavation-induced fracture network around an underground drift: a case study for a radioactive waste repository in clay rock. J. Hydrol. 521, 141–156.

David, C., Robion, P., Menendez, B., 2007. Anisotropy of elastic, magnetic and microstructural properties of the Callovo-Oxfordian argillite. Phys. Chem. Earth 32, 145–153.

Gaucher, E., Robelin, C., Matray, J.M., Négrel, G., Gros, Y., Heitz, J.F., Vinsot, A., Rebours, H., Cassagnabère, A., Bouchet, A., 2004. ANDRA underground research laboratory: interpretation of the mineralogical and geochemical data acquired in the Callovian–Oxfordian formation by investigative drilling. Phys. Chem. Earth, Parts A/B/C 29 (1), 55–77.

Hu, D.W., Zhang, F., Shao, J.F., 2014. Experimental study of poromechanical behavior of saturated claystone under triaxial compression. Acta Geotech 9, 207–214.

Huang, R.Q., Wang, X.N., Chan, L.S., 2001. Triaxial unloading test of rocks and its implication for rock burst. Bull. Eng. Geol. Environ. 60, 37–41.

Le Pense, S., Arson, C., Pouya, A., 2016. A fully coupled damage-plasticity model for unsaturated geomaterials accounting for the ductile–brittle transition in drying clayey soils. Int. J. Solid Struct. 91, 102–114.

Li, D., Sun, Z., Xie, T., Li, X., Ranjith, P.G., 2017. Energy evolution characteristics of hard rock during triaxial failure with different loading and unloading paths. Eng. Geol. 228, 270–281.
Liu, Z., Shao, J., 2016. Moisture effects on damage and failure of Bure claystone under compression. Géotech. Lett. 6 (3), 182–186.
Liu, Z., Shao, J., Xie, S., Conil, N., Talandier, J., 2019. Mechanical behavior of claystone in lateral decompression test and thermal effect. Rock Mech. Rock Eng. 52 (2), 321–334.
Mánica, M., Gens, A., Vaunat, J., Armand, G., Vu, M.N., 2022a. Numerical simulation of underground excavations in an indurated clay using nonlocal regularisation. Part 1: formulation and base case. Geotechnique 72 (12), 1092–1112.
Mánica, M., Gens, A., Vaunat, J., Armand, G., Vu, M.N., 2022b. Numerical simulation of underground excavations in an indurated clay using nonlocal regularisation. Part 2: sensitivity analysis. Geotechnique 72 (12), 1113–1128.
Menaceur, H., Delage, P., Tang, A.M., Talandier, J., 2016. The status of water in swelling shales: an insight from the water retention properties of the Callovo-Oxfordian claystone. Rock Mech. Rock Eng. 49 (12), 4571–4586.
Mohajerani, M., Delage, P., Monfared, M., Tang, A.M., Sulem, J., Gatmiri, B., 2011. Oedometric compression and swelling behaviour of the Callovo-Oxfordian argillite. Int. J. Rock Mech. Min. Sci. 48 (4), 606–615.
Niandou, H., Shao, J.F., Henry, J.P., Fourmaintraux, D., 1997. Laboratory investigation of the mechanical behaviour of Tournemire shale. Int. J. Rock Mech. Min. Sci. 34 (1), 3–16.
Plúa, C., Vu, M.N., de La Vaissière, R., Armand, G., 2024. In situ thermal hydrofracturing behavior of the Callovo-Oxfordian claystone within the context of the deep geological disposal of radioactive waste in France. Rock Mech. Rock Eng. 57 (6), 4265–4283.
Seyedi, D.M., Armand, G., Noiret, A., 2017. "Transverse Action" – a model benchmark exercise for numerical analysis of the Callovo-Oxfordian claystone hydromechanical response to excavation operations. Comput. Geotech. 85, 287–305.
Souley, M., Vu, M.N., Armand, G., 2022. 3D modelling of excavation-induced anisotropic responses of deep drifts at the Meuse/Haute-Marne URL. Rock Mech. Rock Eng. 55 (7), 4183–4207.
Souley, M., Coarita-Tintaya, E.D., Vu, M.N., Golfier, F., Armand, G., Laviña, M., Idiart, A., 2024. A regularised anisotropic elastoplastic damage and viscoplastic model and its hydromechanical application to a Meuse/Haute-Marne URL drift. Rock Mech. Rock Eng. 57 (6), 4389–4419.
Vu, M.N., Guayacán Carrillo, L.M., Armand, G., 2023. Excavation induced over pore pressure around drifts in the Callovo-Oxfordian claystone. Eur. J. Environ. Civ. Eng. 27 (8), 2614–2629.
Wang, L.L., Bornert, M., Héripré, E., Yang, D.S., Chanchole, S., 2014. Irreversible deformation and damage in argillaceous rocks induced by wetting/drying. J. Appl. Geophys. 107, 108–118.
Wang, L.L., Bornert, M., Héripré, E., Chanchole, S., Pouya, A., Halphen, B., 2015. Microscale insight into the influence of humidity on the mechanical behaviour of mudstones. J. Geophys. Res. Solid Earth 120 (5), 3173–3186.
Wang, H., 2021. Delayed and swelling behaviour of damaged/fractured Callovo-Oxfordian claystone. PhD Thesis. École des Ponts ParisTech, France.
Wang, H., Cui, Y.J., Vu, M.N., Talandier, J., Conil, N., 2022. Developing a method for preparing Callovo-Oxfordian claystone samples at a desired damage level in triaxial cell. Rock Mech. Rock Eng. 55 (10), 6103–6119.
Wileveau, Y., Cornet, F.H., Desroches, J., Blumling, P., 2007. Complete in situ stress determination in an argillite sedimentary formation. Phys. Chem. Earth 32, 866–878.
Wileveau, Y., Bernier, F., 2008. Similarities in the hydromechanical response of Callovo-Oxfordian clay and Boom clay during gallery excavation. Phys. Chem. Earth 33, S343–S349.
Yang, D., Chanchole, S., Valli, P., Chen, L., 2013. Study of the anisotropic properties of argillite under moisture and mechanical loads. Rock Mech. Rock Eng. 46, 247–257.
Yu, Z., Shao, J.F., Duveau, G., Vu, M.N., Armand, G., 2021. Numerical modeling of deformation and damage around underground excavation by phase-field method with hydromechanical coupling. Comput. Geotech. 138, 104369.
Zhang, C.L., Rothfuchs, T., 2004. Experimental study of hydromechanical behaviour of the Callovo-Oxfordian argillites. Appl. Clay Sci. 26, 325–336.
Zhang, C.L., Czaikowski, O., Rothfuchs, T., 2010. Thermo-Hydro-Mechanical Behaviour of the Callovo-Oxfordian Clay Rock – Final Report of the EC-TIMODAZ Project. GRS-266.
Zhang, F., Xie, S.Y., Hu, D.W., Shao, J.F., Gatmiri, B., 2012. Effect of water content and structural anisotropy on mechanical property of claystone. Appl. Clay Sci. 69, 79–86.
Zhang, C.L., 2016. The stress–strain–permeability behaviour of clay rock during damage and recompaction. J. Rock Mech. Geotech. Eng. 8 (1), 16–26.
Zhang, C., Armand, G., Conil, N., Laurich, B., 2019. Investigation on anisotropy of mechanical properties of Callovo-Oxfordian claystone. Eng. Geol. 251, 128–145.

Dr. Hao Wang obtained his BSc, MSc, and PhD degrees in Civil Engineering from Shanghai University (China), Geotechnical Engineering from Tongji University (China) and Ecole des Ponts ParisTech (France) in 2014, 2017, and 2021, respectively. His research work includes the laboratory tests of unsaturated soil, thermo-hydro-mechanical constitutive modelling, finite element method, stiff clay/claystone, etc.